Research Article | Vol. 7, No. 8 | 1 Aug 2016 | BIOMEDICAL OPTICS EXPRESS 3032
Biomedical Optics EXPRESS

Phase-stable swept source OCT angiography in human skin using an akinetic source

ZHE CHEN,[1] MENGYANG LIU,[1] MICHAEL MINNEMAN,[2] LAURIN GINNER,[1,3] ERICH HOOVER,[2] HARALD SATTMANN,[1,2] MARCO BONESI,[1] WOLFGANG DREXLER,[1] AND RAINER A. LEITGEB[1,3,*]

[1]*Center of Medical Physics and Biomedical Engineering, Medical University Vienna, Währinger Gürtel 18-20, 1090 Vienna, Austria*
[2]*Insight Photonic Solutions, Inc., 300 S. Public Rd., Lafayette CO 80026, USA*
[3]*Christian Doppler Laboratory for Innovative Optical Imaging and its Translation to Medicine, Währinger Gürtel 18-20, 1090 Vienna, Austria*
[*]*rainer.leitgeb@meduniwien.ac.at*

Abstract: We demonstrate noninvasive structural and microvascular contrast imaging of human skin *in vivo*, using phase difference swept source OCT angiography (pOCTA). The pOCTA system employs an akinetic, all-semiconductor, highly phase-stable swept laser source which operates at 1340 nm central wavelength, with 37 nm bandwidth (at 0 dB region) and 200 kHz A-scan rate. The phase sensitive detection does not need any external phase stabilizing implementations, due to the outstanding high phase linearity and sweep phase repeatability within 2 mrad. We compare the performance of phase based OCTA to speckle based OCTA for visualizing human vascular networks. pOCTA shows better contrast especially for deeper vascular details as compared to speckle based OCTA. The phase stability of the akinetic source allows the OCTA system to show decent vascular contrast only with 2 B-scans. We compare the performance of using 2 versus 4 B-scans for calculating the vascular contrast. Finally, the performance of a 100 nm bandwidth akinetic laser at 1310 nm is investigated for both OCT and OCTA.

OCIS codes: (170.4500) Optical coherence tomography; (170.4580) Optical diagnostics for medicine; (170.3880) Medical and biological imaging; (170.0110) Imaging systems; (140.3600) Lasers, tunable.

References and links

1. W. Drexler and J. G. Fujimoto, "Optical Coherence Tomography -Technology and Applications. 2 ed," Switzerland: Springer International Publishing; 2015.
2. T. E. Carlo, A. Romano, N. K. Waheed, and J. S. Duker, "A review of optical coherence tomography angiography (OCTA)," International Journal of Retina and Vitreous **1**(1), 1–15 (2015).
3. R. A. Leitgeb, R. M. Werkmeister, C. Blatter, and L. Schmetterer, "Doppler Optical Coherence Tomography," Prog. Retin. Eye Res. **41**, 26–43 (2014).
4. R. F. Spaide, J. G. Fujimoto, and N. K. Waheed, "Optical Coherence Tomography Angiography," Retina **35**(11), 2161–2162 (2015).
5. W. Drexler, M. Liu, A. Kumar, T. Kamali, A. Unterhuber, and R. A. Leitgeb, "Optical coherence tomography today: speed, contrast, and multimodality," J. Biomed. Opt. **19**(7), 071412 (2014).
6. X. J. Wang, T. E. Milner, and J. S. Nelson, "Characterization of fluid flow velocity by optical Doppler tomography," Opt. Lett. **20**(11), 1337–1339 (1995).
7. J. A. Izatt, M. D. Kulkarni, S. Yazdanfar, J. K. Barton, and A. J. Welch, "In vivo bidirectional color Doppler flow imaging of picoliter blood volumes using optical coherence tomography," Opt. Lett. **22**(18), 1439–1441 (1997).
8. Y. Zhao, K. M. Brecke, H. Ren, Z. Ding, J. S. Nelson, and Z. Chen, "Three-dimensional reconstruction of in vivo blood vessels in human skin using phase-resolved optical Doppler tomography," IEEE J. Sel. Top. Quantum Electron. **7**(6), 931–935 (2001).
9. S. Makita, Y. Hong, M. Yamanari, T. Yatagai, and Y. Yasuno, "Optical coherence angiography," Opt. Express **14**(17), 7821–7840 (2006).
10. T. Schmoll, C. Kolbitsch, and R. A. Leitgeb, "Ultra-high-speed volumetric tomography of human retinal blood flow," Opt. Express **17**(5), 4166–4176 (2009).

#264314 http://dx.doi.org/10.1364/BOE.7.003032
Journal © 2016 Received 10 May 2016; revised 30 Jun 2016; accepted 7 Jul 2016; published 12 Jul 2016

Biomedical Optics EXPRESS

11. I. Grulkowski, I. Gorczynska, M. Szkulmowski, D. Szlag, A. Szkulmowska, R. A. Leitgeb, A. Kowalczyk, and M. Wojtkowski, "Scanning protocols dedicated to smart velocity ranging in spectral OCT," Opt. Express **17**(26), 23736–23754 (2009).
12. A. Mariampillai, B. A. Standish, E. H. Moriyama, M. Khurana, N. R. Munce, M. K. K. Leung, J. Jiang, A. Cable, B. C. Wilson, I. A. Vitkin, and V. X. D. Yang, "Speckle variance detection of microvasculature using swept-source optical coherence tomography," Opt. Lett. **33**(13), 1530–1532 (2008).
13. C. Blatter, T. Klein, B. Grajciar, T. Schmoll, W. Wieser, R. Andre, R. Huber, and R. A. Leitgeb, "Ultrahigh-speed non-invasive widefield angiography," J. Biomed. Opt. **17**(7), 070505 (2012).
14. K. K. C. Lee, A. Mariampillai, J. X. Z. Yu, D. W. Cadotte, B. C. Wilson, B. A. Standish, and V. X. D. Yang, "Real-time speckle variance swept-source optical coherence tomography using a graphics processing unit," Biomed. Opt. Express **3**(7), 1557–1564 (2012).
15. J. Xu, K. Wong, Y. Jian, and M. V. Sarunic, "Real-time acquisition and display of flow contrast using speckle variance optical coherence tomography in a graphics processing unit," J. Biomed. Opt. **19**(2), 026001 (2014).
16. D. Y. Kim, J. Fingler, J. S. Werner, D. M. Schwartz, S. E. Fraser, and R. J. Zawadzki, "In vivo volumetric imaging of human retinal circulation with phase-variance optical coherence tomography," Biomed. Opt. Express **2**(6), 1504–1513 (2011).
17. D. M. Schwartz, J. Fingler, D. Y. Kim, R. J. Zawadzki, L. S. Morse, S. S. Park, S. E. Fraser, and J. S. Werner, "Phase-variance optical coherence tomography: a technique for noninvasive angiography," Ophthalmology **121**(1), 180–187 (2014).
18. R. F. Spaide, J. G. Fujimoto, and N. K. Waheed, "Image artifacts in optical coherence tomography angiogrpahy," Retina **35**(11), 2163–2180 (2015).
19. M. S. Mahmud, D. W. Cadotte, B. Vuong, C. Sun, T. W. Luk, A. Mariampillai, and V. X. Yang, "Review of speckle and phase variance optical coherence tomography to visualize microvascular networks," J. Biomed. Opt. **18**(5), 050901 (2013).
20. L. An, J. Qin, and R. K. Wang, "Ultrahigh sensitive optical microangiography for in vivo imaging of microcirculations within human skin tissue beds," Opt. Express **18**(8), 8220–8228 (2010).
21. T. Schmoll, I. R. Ivascu, A. S. G. Singh, C. Blatter, and R. A. Leitgeb, "Intra-and inter-frame differential Doppler optical coherence tomography," Sovremennye Tehnologii v Medicine **7**, 34–42 (2015).
22. D. D. John, C. B. Burgner, B. Potsaid, M. E. Robertson, B. K. Lee, W. J. Choi, A. E. Cable, J. G. Fujimoto, V. Jayaraman, "Wideband Electrically-Pumped 1050 nm MEMS-Tunable VCSEL for Ophthalmic Imaging," J. Lightwave Technol. **33**, 3461–3468 (2015).
23. I. Grulkowski, J. J. Liu, B. Potsaid, V. Jayaraman, J. Jiang, J. G. Fujimoto, and A. E. Cable, "High-precision, high-accuracy ultralong-range swept-source optical coherence tomography using vertical cavity surface emitting laser light source," Opt. Lett. **38**(5), 673–675 (2013).
24. R. Huber, M. Wojtkowski, and J. G. Fujimoto, "Fourier Domain Mode Locking (FDML): A new laser operating regime and applications for optical coherence tomography," Opt. Express **14**(8), 3225–3237 (2006).
25. T. Klein, W. Wieser, L. Reznicek, A. Neubauer, A. Kampik, and R. Huber, "Multi-MHz retinal OCT," Biomed. Opt. Express **4**(10), 1890–1908 (2013).
26. M. Bonesi, M. P. Minneman, J. Ensher, B. Zabihian, H. Sattmann, P. Boschert, E. Hoover, R. A. Leitgeb, M. Crawford, and W. Drexler, "Akinetic all-semiconductor programmable swept-source at 1550 nm and 1310 nm with centimeters coherence length," Opt. Express **22**(3), 2632–2655 (2014).
27. R. F. Stancu and A. G. Podoleanu, "Dual-mode-locking mechanism for an akinetic dispersive ring cavity swept source," Opt. Lett. **40**(7), 1322–1325 (2015).
28. W. Choi, B. Potsaid, V. Jayaraman, B. Baumann, I. Grulkowski, J. J. Liu, C. D. Lu, A. E. Cable, D. Huang, J. S. Duker, and J. G. Fujimoto, "Phase-sensitive swept-source optical coherence tomography imaging of the human retina with a vertical cavity surface-emitting laser light source," Opt. Lett. **38**(3), 338–340 (2013).
29. B. Braaf, K. A. Vermeer, V. A. D. P. Sicam, E. van Zeeburg, J. C. van Meurs, and J. F. de Boer, "Phase-stabilized optical frequency domain imaging at 1-μm for the measurement of blood flow in the human choroid," Opt. Express **19**(21), 20886–20903 (2011).
30. B. Vakoc, S. Yun, J. de Boer, G. Tearney, and B. Bouma, "Phase-resolved optical frequency domain imaging," Opt. Express **13**(14), 5483–5493 (2005).
31. C. Blatter, J. Weingast, A. Alex, B. Grajciar, W. Wieser, W. Drexler, R. Huber, and R. A. Leitgeb, "In situ structural and microangiographic assessment of human skin lesions with high-speed OCT," Biomed. Opt. Express **3**(10), 2636–2646 (2012).
32. U. Baran, W. J. Choi, R. K. Wang, "Potential use of OCT-based microangiography in clinical dermatology," Skin research and technology: official journal of International Society for Bioengineering and the Skin (ISBS) [and] International Society for Digital Imaging of Skin (ISDIS) [and] International Society for Skin Imaging (ISSI) 2015.
33. A. Bachmann, R. Leitgeb, and T. Lasser, "Heterodyne Fourier domain optical coherence tomography for full range probing with high axial resolution," Opt. Express **14**(4), 1487–1496 (2006).
34. Z. Chen, T. E. Milner, S. Srinivas, X. Wang, A. Malekafzali, M. J. van Gemert, and J. S. Nelson, "Noninvasive imaging of in vivo blood flow velocity using optical Doppler tomography," Opt. Lett. **22**(14), 1119–1121 (1997).

Biomedical Optics EXPRESS

35. R. Leitgeb, L. Schmetterer, W. Drexler, A. Fercher, R. Zawadzki, and T. Bajraszewski, "Real-time assessment of retinal blood flow with ultrafast acquisition by color Doppler Fourier domain optical coherence tomography," Opt. Express **11**(23), 3116–3121 (2003).
36. B. White, M. Pierce, N. Nassif, B. Cense, B. Park, G. Tearney, B. Bouma, T. Chen, and J. de Boer, "In vivo dynamic human retinal blood flow imaging using ultra-high-speed spectral domain optical coherence tomography," Opt. Express **11**(25), 3490–3497 (2003).
37. J. Zhang and Z. Chen, "In vivo blood flow imaging by a swept laser source based Fourier domain optical Doppler tomography," Opt. Express **13**(19), 7449–7457 (2005).
38. R. C. Gonzalez and R. E. Woods, *Digital Image Processing*, 3rd ed. (Prentice Hall: Upper Saddle River, NJ, USA, 2008).
39. Eucerin, http://m.int.eucerin.com/skin-concerns/ageing-skin/wrinkles.

1. Introduction

Optical coherence tomography angiography (OCTA) is currently the most successful functional extension of OCT, due to the fact that it can be implemented in any OCT platform and it meets an immediate clinical diagnostic need [1–4]. OCT intensity data alone provides high contrast and sensitivity, but misses important tissue specificity as well as valuable physiological information [5]. The latter is provided by functional extensions of OCT, such as Doppler OCT (DOCT) to assess blood flow [6]. It has already been shown with early Time Domain OCT (TD-OCT) that DOCT is able to assess blood flow quantitatively as well as using the flow signature to contrast vascular structure [6–8]. However, only with the advent of high-speed Fourier domain OCT (FDOCT), the full potential of DOCT to perform non-invasive volumetric angiography was unleashed [9,10]. Based on OCT spectral data alone, OCTA provides vascular structure with unprecedented resolution and detail down to the level of individual capillaries in a fully non-invasive and label-free manner. Hence, one has not only co-registered anatomical structure but also vascular structure from OCT.

The working principle of OCTA is to sense dynamic structural changes in-between successive tomograms [11]. The simplest approach is to calculate the average of pairwise differences of a set of linearly or logarithmically scaled intensity tomograms taken at the same position [12,13]. We will refer to this method as intensity based OCTA (iOCTA). Further, implementation on a graphics processing unit (GPU) based system allows real time visualization of volumetic angiograms [14,15]. Alternatively, one can use the phase information of the FDOCT signal obtained after the Fourier transform of spectral data [16,17]. Again, the motion contrast is achieved by taking the average of pairwise phase differences across a set of phase tomograms at the same position. Still, phase is highly sensitive to motion in the sub-wavelength region, which results in stripe-like B-scan motion artifacts that obstruct the vascular structure [18]. Therefore, it is necessary to correct bulk motion prior to motion contrasting, especially for *in-vivo* measurements, which increases the post-processing effort. This method is subsequently referred to phase-sensitive OCTA (pOCTA). The advantage of pOCTA is its independency of backscattering intensity changes, yielding potentially better vascular contrast for highly scattering tissue [19]. A hybrid of both methods is to calculate differences of the full complex OCT signal or of spectral data [20,21]. The latter, also termed OCT-based micro-angiography (OMAG), has shown high contrast for both low scattering and highly scattering tissue; but like pOCTA, it needs bulk motion correction prior to motion contrast analysis. Both pOCTA and cOCTA (complex spectral OCTA) are easily adapted to spectral OCT devices, which record whole A-scans in single camera shots, thereby achieving high system phase stability. Swept source OCT (SSOCT), on the other hand, becomes increasingly popular, due to its potentially more compact fiber-based setup, its higher speed, better signal to noise ratio (SNR) and the depth performance with respect to ranging depth and sensitivity [1,5]. Also, SSOCT operates in the longer wavelength region, where scattering is less pronounced. Recent advancements of laser technology such as VCSEL sources [22,23], FDML lasers operating in the MHz range [24,25] and akinetic lasers [26,27] increase further its attractiveness.

Biomedical Optics EXPRESS

However, in case of swept source pOCTA, dedicated hardware such as fiber Bragg gratings, reference interferometers and sophisticated post-processing routines are necessary to ensure a wavelength-stable sampled signal [28,29]. Any trigger jitter could deteriorate the signal phase and result in errors in depth dependent phase, which are hard to be eliminated in post-processing alone [30]. Currently, most pOCTA and cOCTA systems are based on spectral OCT because of the reduced system complexity.

Recently, akinetic swept source technology has been introduced, which provides precise electronic control of the spectral laser output over time. Its principle is based on Vernier tuning of the laser cavity and has been explained in detail earlier [26]. The laser using this technology combines high instantaneous coherence length of 10 times of centimeters with extremely high wavelength stability (phase repeatability standard deviation of <2 mrad); besides, it produces low excess noise. Especially the tuning stability holds great promise for phase sensitive OCT modalities such as pOCTA and cOCTA. First reported lasers were centered at 1550 nm and 1340 nm with respective bandwidths of 40 nm and 30 nm. The wavelength of 1300nm is commonly used for imaging scattering tissue like skin, brain tissue or internal organs. Investigations about skin based on OCTA demonstrated its high clinical relevance for diagnosis of common diseases, e.g. basal cell carcinoma or psoriasis [31], as well as for treatment monitoring and wound healing [32].

In the present work we will perform OCTA in human skin *in-vivo* with a 1340 nm akinetic laser to demonstrate its ability. We show that the intrinsic wavelength stability of the akinetic source enables phase-stable recording of spectral SSOCT data without any additional hardware or post-processing, which could substantially increase the imaging speed and reduce the complexity of computation hardware in deployed systems. The phase based OCTA using the 1340 nm akinetic laser in this paper is referred as pOCTA. Then we compare the performance of iOCTA and pOCTA demonstrating the superior performance of phase based OCTA in deep tissue. Furthermore, we analyze the impact of the higher phase stability of the akinetic laser on the number of necessary tomograms used to calculate the motion contrast volumes, as well as using 37 nm and 100 nm bandwidth (note that sweep rates in INSIGHT lasers indicate linear tuning range) centered at 1340 nm and 1310 nm.

2. Method

In the following sections we will present the setup of pOCTA system and the principles of the post-processing procedures of pOCTA in the system. Further, we will show the principles of the intensity based and the phase based OCTA, respectively.

2.1 Setup

The setup of the pOCTA system is shown in Fig. 1(a). The system employs a 1340 nm central wavelength swept source (SSOCT-1340, Insight Photonic Solutions, Inc, U.S.) with a maximum bandwidth of 37 nm and a sweep repetition rate of 200 kHz (the repetition rate is programmable and can be set from 20 kHz to 200 kHz across the full wavelength range and up to 400 KHz across an reduced range). The output power of the laser is 12 mW and the spectrum profile is extremely flat along the whole sweeping range (the variation is within 0.015dB). The power incident upon the sample was measured to be 6.2 mW. A 2D pixel-by-pixel scan over the sample is enabled by two scanning mirrors (6210H, Cambridge Technology), whose scanning pattern was controlled by the analog output of a FPGA (NI PCIE-7841R, National Instruments). The interference signal is measured by a dual balanced photodetector (DBP) (Insight Photonic Solutions, 950-1650 nm detection wavelength, 400 MHz band pass) and amplified by a pre-amplifier (NI PXI 5690). The data was acquired by a digitizer (AlazaTech, ATS9360, 1.8 GS/s sample rata digitalizer) at 400 MS/s from the AC channel of the photodiode. The lateral and axial resolution were experimentally determined by imaging a resolution target and a mirror, to be 45.67 μm and 26.86 μm in air, respectively.

Biomedical Optics EXPRESS

By using a neutral density filter (OD = 2) in the sample arm and a mirror as sample, a sensitivity of 103 dB was measured by calculating the SNR.

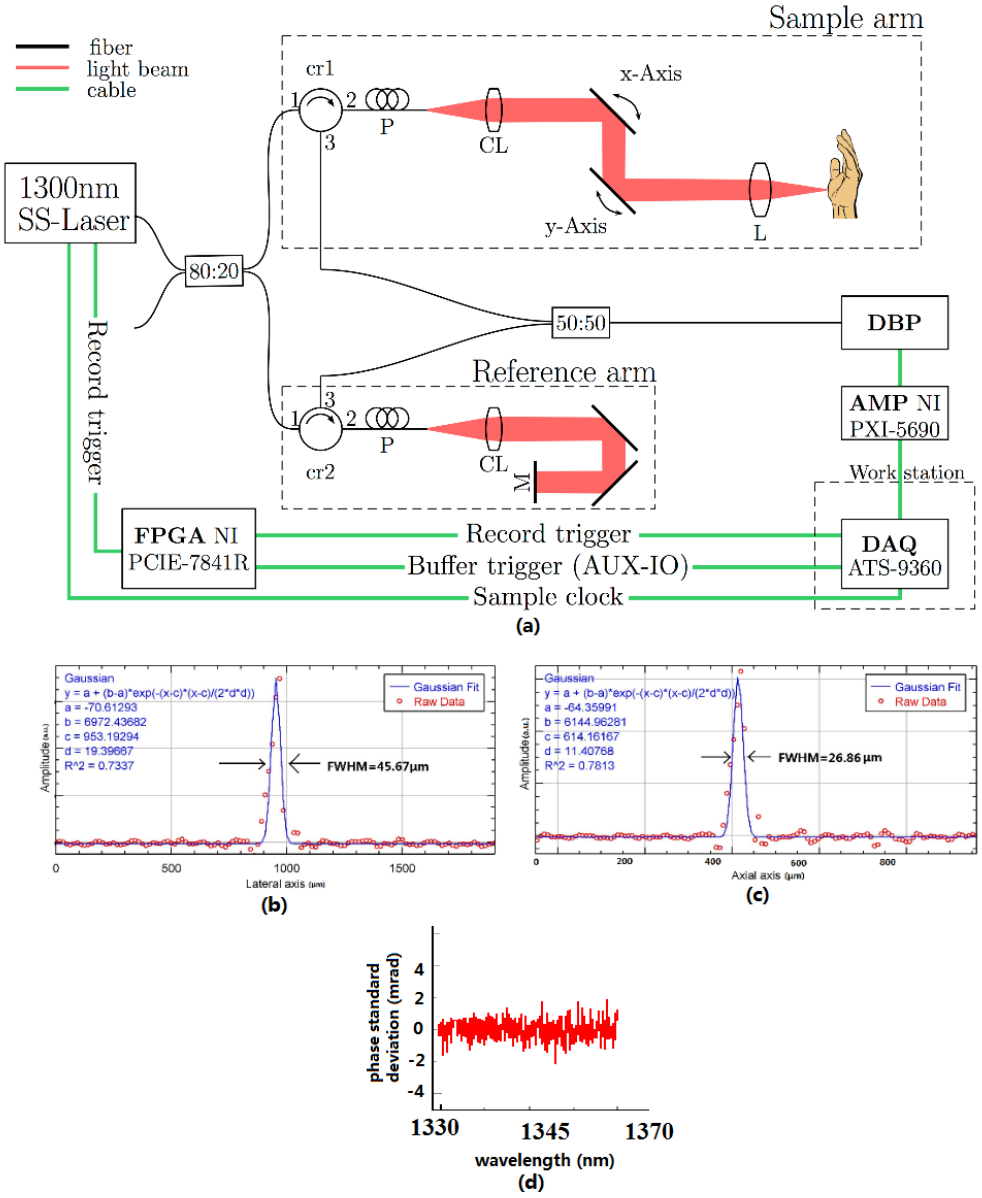

Fig. 1. (a) Schematic representation of the imaging setup as used in the experiments. 80:20 – fiber-based single mode optical coupler, 80/20 splitting ratio; cr1, cr2 – circulator; p – polarization controller; c – collimator; R – retroreflector; M – mirror; x, y scan – 2-axis galvo-scan unit; L – imaging lens; DBP – dual-balanced photodetector; AMP – pre-amplifier; DAQ – data acquisition card. (b) full width at half maximum (FWHM) represents the lateral resolution of the system by measuring the edge spread function of a resolution target and then Gaussian fitting. (c) FWHM represents the axial resolution in air by measuring the line spread function of a mirror and then Gaussian fitting. (d) phase standard deviation (in 15 seconds) of the whole sweep.

Note that there is neither a reference interferometer nor fiber Bragg grating necessary to guarantee phase-stable tuning and data acquisition. The phase stability is intrinsic to the

Biomedical Optics EXPRESS

working principle of the akinetic laser source. The laser directly supplies a uniform in time and frequency user sample clock (or electronic k-clock) signal and a start-sweep (A-line trigger) signal for convenient integration of the laser source into the SS-OCT system and optimal synchronization with data acquisition hardware. It significantly simplifies the system regarding to hardware and the post-processing routines for phase sensitive OCT signal analysis. During the experiments, robustness and wide customizability were experienced, allowing the user to select and/or adjust the central laser parameters, including laser output power, spectral bandwidth and sweep rate. For the present work the spectral bandwidth as well as sweep rate were held constant at 37 nm and 200 kHz, respectively. To evaluate the laser's sweep phase stability, auto-correlation measurement were performed. A set of consecutive spectra (sweeps) were collected from the same point on the sample (no xy scan active) using a 1 mm thick cover glass as sample in the sample arm, with the sample arm focal plane positioned inside the cover glass just beyond the front surface. Data was obtained with the reference arm signal blocked while recording the self-interfering signal (front surface of the cover glass referred to its back surface) generated from the sample arm. Assuming that the self-interfered signal did not experience significant disturbances in the phase when travelling outside the laser source, the computed phase variations with auto-correlation analysis are attributed mainly to overall phase variations arising inside the laser source. The measurement took 15 seconds and all the data was taken to calculate the phase standard deviation. It can be seen in Fig. 1(d) that the phase standard deviation in 15 seconds of the whole sweep range is smaller than 2 mrad. The detailed measuring procedure of phase repeatability is written in our previous work [26].

2.2 Principles of post-processing of OCT Angiography

The operating principle of the akinetic source was explained in detail previously [26]. The laser produces 400 million wavenumber points/second resulting in 2048 spectral sampling points at 200 kHz sweep rate. However, those points do not define a linear ramp in wavenumber space, due to the tuning principle of the laser. The sweep consists of sub-intervals interspersed by transition intervals where the laser parameters are readjusted. In order to properly interpret the sampled spectral data, the laser delivers a table of valid and invalid states. As described previously [26] the laser has multiple optical and electronic feedback mechanisms to optimize sweep performance. After the intial optimization, that needs to be performed only once for the laser, 1643 valid data points are provided, that yield a spectrum sampled linearly in k. This number of valid data points for each sweep stays fixed for all experiments with the laser source. A simple fast Fourier transform (FFT) of the spectral data without k-mapping yields then an OCT A-scan as a function of depth. Prior to FFT, subtraction of a background signal is applied, where the background has been calculated as average spectrum across a recorded tomogram. The FFT yields intensity and phase information, which are both used for the angiography algorithms explained below.

2.2.1 Intensity based OCT angiography (iOCTA)

The iOCTA, also known as speckle based OCT angiography, operates on the intensity of the Fourier transformed OCT signal, namely, the magnitude of the Fourier transform of the interference signal $\mathrm{FFT}\left[S(x,k)\right]=\mathrm{T}(x,z)exp\left[-i\varphi(x,z)\right]$. A key advantage of the iOCTA is that it is relatively less sensitive to phase noise and trigger jitter, making it particularly helpful in situations where the phase stability of the light source is an issue. Due to its robustness and easy implementation it is preferably used for swept source OCT angiography. Common to all angiography methods is the scanning principle of recording a set of several tomograms along the fast scanning direction at a given position of the sample before stepping along the slow scanning direction to the next position. The motion contrast volume $\mathrm{A}(x,y,z)$ is obtained by averaging over pairwise differences of subsequent logarithmically-

Biomedical Optics EXPRESS

scaled intensity tomograms log(T(x,z)) from the same set at given position y. The tomograms are axially registered prior to subtraction using a simple cross-correlation technique. It is calculated as:

$$A(x,y,z)=\frac{1}{N-1}\sum_{i=0}^{N-1}\left|log\left(T(x,z)_{i+1}\right)-log\left(T(x,z)_{i}\right)\right|\Big|_{\substack{set\ of\ N\ tomograms\\ taken\ at\ y}} \quad (1)$$

where N is the number of B-scans repetition (in this work: 2 and 4), (x,z) are the spatial pixel coordinates in the fast scan direction and depth, respectively and i denotes the B frame slice index within N. Therefore, $T(x,z)_i$ is the i'th 2-D intensity tomogram of the set of N tomograms at a single slow axis position.

2.2.2 Phase based OCT angiography (pOCTA)

The phase signal is immediately available as argument of the FFT of the spectral interference pattern, $\varphi(x,z)=\arg FFT\left[S(x,k)\right]$. Motion contrast is achieved as blood flow induced decorrelation of the OCT phase signal. Since the phase is sensitive to axial sub-wavelength displacement of the sample, correction of bulk motion is required for in-vivo measurements. Again, a set of N spectral tomograms $\left[S(x,k)\right]$ is recorded sequentially for each slow scanning position y. Firstly, the phase differences between two A-scans at the same position, but of consecutive B-scans are calculated as $\Delta\varphi(x,z)_i=arg\left\{exp\left[-i\varphi(x,z)_{i+1}\right]exp\left[i\varphi(x,z)_i\right]\right\}$, where the index i denotes the tomogram within the set of N tomograms taken at the same position y. After the calculation of the phase difference between A-scans of consecutive B-scans, the phase difference between consecutive B-scans is achieved. Then, the circularly averaged phase difference $\overline{\Delta\phi}(x)_i$ is calculated for each lateral position x in the i-th phase difference tomogram. Bulk motion is then corrected by subtracting $\overline{\Delta\phi}(x)_i$ along the A-scan within the (i + 1)-th phase difference tomogram at the respective positions x. Motion contrast is finally achieved by averaging over the set of bulk motion corrected phase difference tomograms taken at the same location y as:

$$A(x,y,z)=\frac{1}{N-1}\sum_{i=0}^{N-1}\left|\Delta\varphi(x,z)_i\right|\Big|_{\substack{set\ of\ N\ tomograms\\ taken\ at\ y}} \quad (2)$$

where N is the number of B-scans repetition, and (x,z) are the spatial pixel coordinates in the fast scanning direction and depth, respectively. The index i denotes the B frame slice within N. Therefore, $\Delta\varphi(x,z)_i$ is the i'th 2-D phase difference tomogram at position y along the slow axis. Note that $\Delta\varphi(x,z)_i$ is the data after bulk motion correction as we mentioned above. For producing *en-face* OCTA images, the median of the OCTA signal along a selected depth interval is calculated and plotted for each lateral point. It has been empirically found, that calculating the median yields a better vascular contrast than calculating the mean signal or performing a maximum intensity projection.

The post-processing effort for pOCTA is obviously higher than for iOCTA. The main advantage of the pOCTA is the independency of the intensity which should potentially yield better contrast in situations of strong backscattering.

Biomedical Optics EXPRESS

3. Results and discussion

The pOCTA system operates at a 1340 nm central wavelength with a bandwidth of 37 nm and a sweep repetition rate of 200 kHz. The recorded volume size is 2048 (number of pixel per A-line) × 512 × 512 pixel for all data sets. Two and four tomograms, respectively, are taken at the same position each time to calculate the respective OCTA volumes and to compare the performance for contrasting the microvascular network in section 3.4. The sample is the hand palm skin and the nail fold region of a healthy volunteer. To demonstrate the phase stability of the system, phase difference tomograms of a piece of rubber as a static homogeneously scattering phantom are acquired first. Furthermore, we evaluate and compare the imaging performance for human vascular networks of iOCTA versus pOCTA (section 2.2). The performances of a 37 nm bandwidth laser and a 100 nm bandwidth laser are also compared.

3.1 Phase difference maps with static scattering phantom

The static rubber phantom was placed in the sample arm and volume data was recorded. Phase difference of tomograms are calculated in order to test the phase stability of the akinetic laser. Figure 2(a) shows the OCT tomogram of the homogenously scattering rubber phantom along the fast scanning direction and Fig. 2(b) shows the phase difference plot along the slow scanning direction. The phase difference values in Fig. 2(b) are displayed only when the associated intensity values in Fig. 2(a) at the same pixel location are above a defined threshold, otherwise the pixel color is set to grey. The threshold is set to −30dB below the maximum intensity value, determined empirically for better visual contrast between actual phase and background noise. The phase difference tomogram shows the excellent intrinsic phase stability of the system. There is no visible deviation from zero phase difference as expected for a static sample. The protocol of calculating phase differences along the slow scanning direction between consecutive B-scans is sensitive to any phase or trigger jitter. The standard deviation across the indicated region-of-interest (ROI) in Fig. 2(b) yielded 80 mrad or 4.58 degrees. Comparing with the phase standard deviation published by Jun Zhang (48°, 840 mrad) [37], the akinetic INSIGHT laser performs with superior phase stability, which is achieved without any additional hardware thanks to the intrinsic precise electronic control of the source itself.

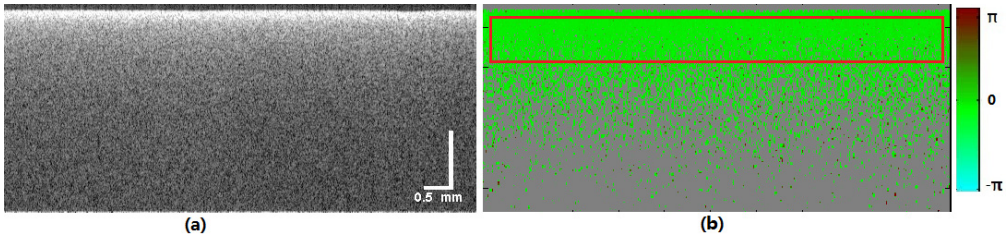

Fig. 2. Tomogram and phase difference with static phantom (rubber) (a) tomogram (512 pixels × 226 pixels, 8 mm × 3.5 mm). (b) phase difference (in radian) of consecutive two tomogram at same position (radian of phase difference is between $-\pi$ and π). The red rectangle indicates the ROI for the phase stability analysis.

3.2. Phase based OCT angiography (pOCTA) in human skin

For the measurement, a healthy volunteer puts his palm against a glass window in the sample arm, which helped stabilization. A drop of water was used for index matching between glass plate and skin surface. Figure 3(a) shows a photograph of the exact measurement location and scan area (8 mm × 8 mm) as well as a typical OCT tomographic cross-section in Fig. 3(b). In Fig. 3(c), the anatomic structure of human skin [39] is presented for better comparison. The motion contrast algorithms are sensitive to both, flowing blood cells in the human vascular network, as well as bulk motion caused by the pulse induced motion of the palm. In the post

Biomedical Optics EXPRESS

processing program (sec 2.2.2), the bulk motion is eliminated by bulk motion correction based on determining the average phase difference, which is dominated by the static tissue motion artifact. In Fig. 3(d) to 3(g), the angiograms show the *en-face* view of the vascular network at different depths (210-235 µm, 294-587 µm, 587-839 µm, 839-1007 µm from the tissue surface). The ranges are indicated in Fig. 3(b) with the letters referring to the *en-face* projections in the respective sub-images of Fig. 3(d), 3(e), 3(f) and 3(g). The data are acquired and post-processed with LabVIEW 2013. The median projection is calculated in ImageJ 1.50f. Further processing steps involve a 1-pixel width Gaussian filter and ImageJ "red hot"-look-up-table for color coding the motion contrast values. The size of the angiogram is 8 mm × 8 mm, sampled by 512 × 512 pixels. In Fig. 3(d), there are clouds of discrete small dots visible, which correspond to horizontally cut capillary loops in the dermis-epidermis junction. These small capillary are almost perpendicular to the surface of the human skin, therefore the small capillary cross sections appear like clouds of dots in the *en-face* view. Figure 3(e) visualizes well the deeper planar vessel network feeding the capillary loops. At larger depth, as seen in Fig. 3(f) and 3(g), vessel networks with increasing diameter are present. Figure 3(h) shows the 3D rendering of angiograms (depth range: 294-1007 µm). These results demonstrate the excellent performance of OCTA for the visualization of capillaries and the vascular network in human skin and gives both reliable morphologic and functional information of skin.

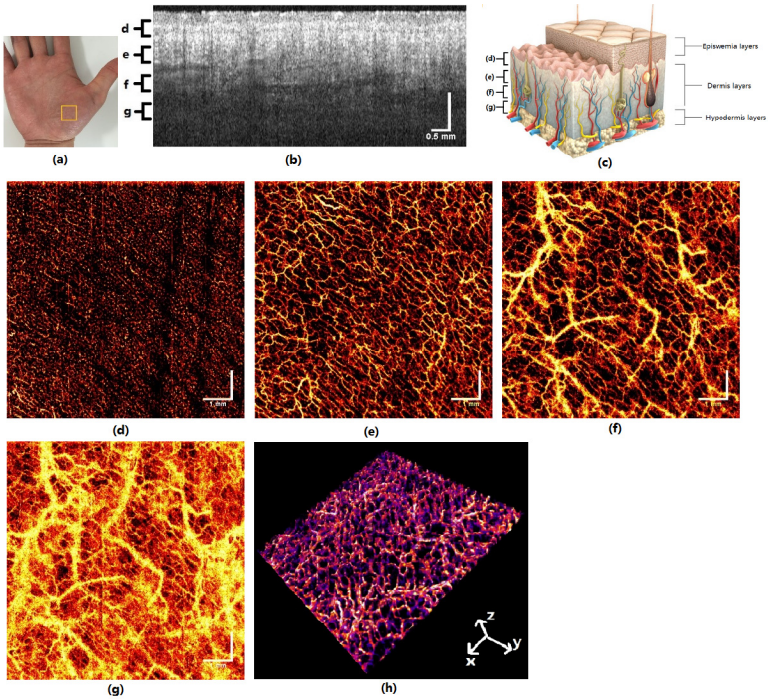

Fig. 3. Tomogram and OCT angiograms based on phase signal at different depths. (a) healthy human palm (b) tomogram (8 × 8mm). (c) structure of skin [39]. (d)-(g) *en-face* view of z-projection of given depth (8 × 8mm, 512 × 512 pixels). (d) 210-235 µm. (e) 294-587 µm. (f) 587-839 µm. (g) 839-1007 µm. (h) 3-D rendering of angiographic volume (depth range: 294-1007 µm) (movie see Visualization 1).

3.3 Phase based OCT angiography (pOCTA) in finger nail

The healthy volunteer pressed the nail fold region of finger against a glass window in the sample arm, which helped stabilization. Figure 4(a) shows a photograph of the exact measurement location at the fingertip and the scan area indicated by the yellow box (8 mm ×

Biomedical Optics EXPRESS

8 mm) as well as a representative OCT tomographic cross-section in Fig. 4(b). For speckle reduction ten successive tomograms were averaged. In Fig. 4(c) to 4(f), the angiograms show *en-face* views of the vascular network at different depths (295-442 µm, 442-590 µm, 590-885 µm, 885-1007 µm respectively). All the angiograms are obtained by median z-projection, Gaussian filtering with kernel pixel size 0.8 and choosing the "red hot" look-up table of ImageJ. In Fig. 4(c), the good contrast for visualizing the microvascular network is well appreciated. In Fig. 4(d) and 4(e), the capillary loops that enter the nail fold are well distinguishable as they run at this position parallel to the surface. Those capillaries are in fact optically accessible by capillaroscopy, for detecting early signs of vascular pathologies, as in case of diabetes. The capillaries beneath the fingernail can be seen in the right side of Fig. 4(f). Figure 4(g) shows the 3D rendering of the full OCT angiography data and Fig. 4(h) indicates the fused 3D rendered angiogram and photograph for better anatomical orientation. The capillaries and vascular network in the finger nail fold region are visualized with high contrast, showing also the deeper vascular network supplying the capillaries. These results meet an immediate clinical diagnostic need [1–4], such as the diagnosis of diabetes and early detection of diabetes induced vascular disorders.

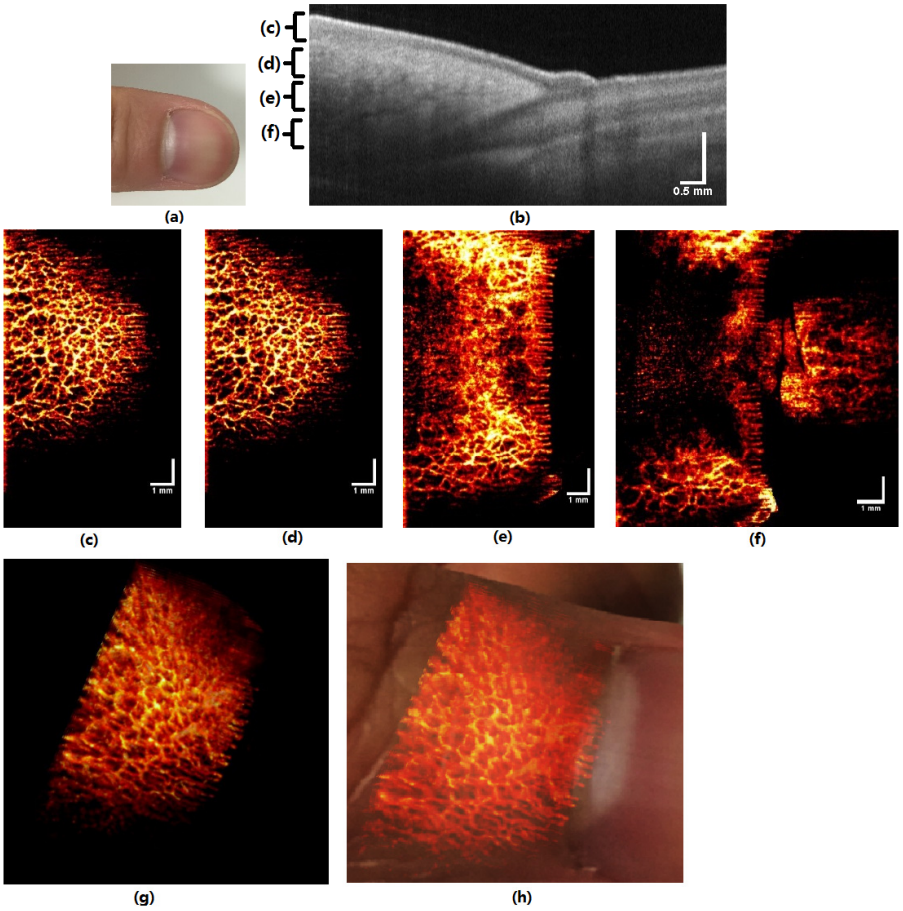

Fig. 4. Tomogram and OCT angiograms of finger nail region based on phase difference signal at different depths. (a) healthy human finger nail, the direction of the finger is the same as tomogram and angiogram. (b) tomogram. (c)-(f) *en-face* view of z-projection of given depth from top surface. (c) 295-442 µm. (d) 442-590 µm. (e) 590-885 µm. (f) 885-1007 µm. (g) 3-D rendering of angiographic volume (movie see Visualization 2). (h) fusion of 3-D rendering of angiographic volume and finger.

Biomedical Optics EXPRESS

3.4 Comparison of speckle based OCT angiography and phase based OCT angiography

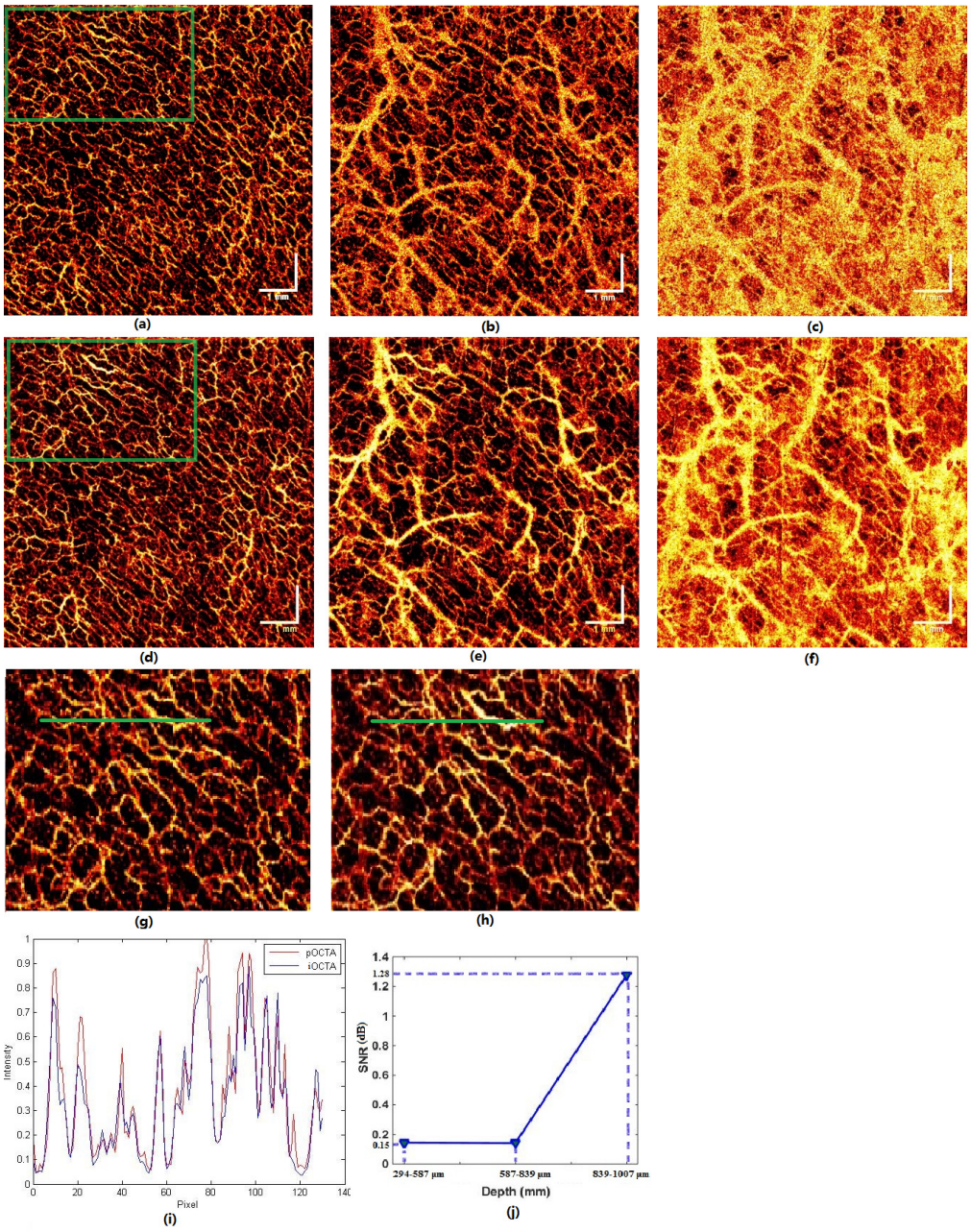

Fig. 5. Comparison of speckle based angiography vs. phase based angiography of healthy human hand palm. (a), (b), (c) speckle based angiograms at different depths (294-587 μm. 587-839 μm and 839-1007 μm respectively), the size of all angiograms is 8 mm × 8 mm and 512 × 512 pixels. (d), (e), (f), phase based angiograms at the same depths like speckle based angiograms (294-587 μm, 587-839 μm and 839-1007 μm respectively). (g) zoom in the dashed rectangle in (a). (h) zoom in the rectangle in (d). (i) profile plotted along the green line in (g) and (h), where the increase of SNR in case of pOCTA can be verified. (j) improvement of SNR at three depths.

Biomedical Optics EXPRESS

The images of (a), (b), (c) in Fig. 5 correspond to speckle (intensity) based OCTA and the images of (d), (e), (f) in Fig. 5 correspond to the pOCTA algorithm. The algorithms are described in detail in section 2.2. Both algorithms operate on the same data set in order to ensure the comparability of the two techniques. All the angiograms employ median z-projection, Gaussian filtering with kernel pixel size 0.8 and "red hot" look-up table. For better comparison, both angiograms have been normalized to the maximum value within an *en-face* image, and the same contrast adjustment (the minimum displayed value and maximum displayed value) in ImageJ has been applied. Figure 5(a) and 5(d), 5(b) and 5(e), 5(c) and 5(f) show the angiograms of iOCTA and pOCTA for different depths (294-587 μm, 587-839 μm and 839-1007 μm respectively). Figure 5(g) and Fig. 5(h) are zoomed in areas of the rectangle indicated in (a) and (d). Figure 5(i) plots the profiles along the green lines in (g) and (h). The peaks, that correspond vessel cross sections, are in most cases higher for the pOCTA profile than the peaks originating from the iOCTA profile plot. In order to quantify the increase in SNR, we compare the angiograms obtained with the intensity based OCTA and phase based OCTA using the following formula for the relative image SNR [38]:

$$SNR = 10 * \log\left[\frac{\sum_{0}^{n_x-1}\sum_{0}^{n_y-1}\left[r(x,y)\right]^2}{\sum_{0}^{n_x-1}\sum_{0}^{n_y-1}\left[r(x,y)-t(x,y)\right]^2}\right] \tag{3}$$

with $\boldsymbol{r}$ being the reference image and t the test image.$\boldsymbol{n}_x$ and $\boldsymbol{n}_y$ are image pixels in the fast scanning and slow scanning direction, respectively. We calculated an improvement of 0.15 dB in SNR for Fig. 5(d), as compared to Fig. 5(a); an improvement of 0.14 dB in SNR for Fig. 5(e), as compared to Fig. 5(b); an improvement of 1.28 dB in SNR for Fig. 5(f), as compared to Fig. 5(c). The improvement of SNR over three depth is shown in Fig. 5(j). pOCTA yields obviously better contrast than iOCTA in terms of SNR which has been observed also by other authors. At shallow depth (294-587 μm, 587-839 μm), the difference of SNR between pOCTA and iOCTA is small, but becomes larger with increasing depth and increasing amount of multiply scattered light. At deeper depth (839-1007 μm), the SNR of pOCTA is much higher than iOCTA reaching up to 1.28 dB. As seen from Fig. 5(c) and 5(f), the contrast is significantly lower for iOCTA.

Biomedical Optics EXPRESS

3.5 Comparison of 2 B-scans and 4 B-scans per position using phase based OCT angiography

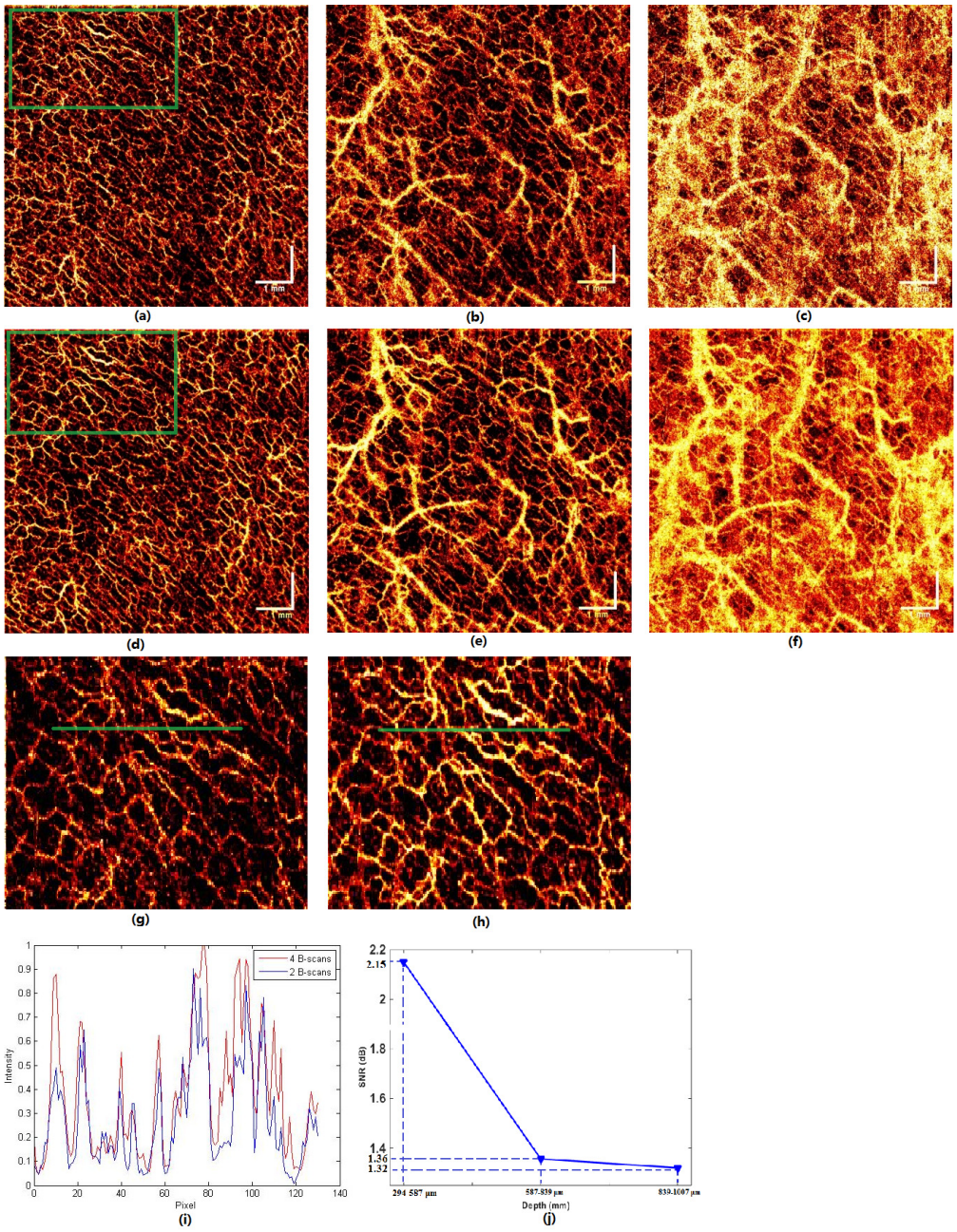

Fig. 6. Comparison of 2 B-scans vs. 4 B–scans based on phase based angiography of healthy human palm. (a), (b), (c) 2 B-scans phase based angiograms at different depths (294-587 µm, 587-839 µm and 839-1007 µm respectively), the size of all angiograms is 8 mm × 8 mm, 512 × 512 pixels. (d), (e), (f), 4 B-scans phase based angiograms at the same depths like 2 B-scans phase based angiograms (294-587 µm, 587-839 µm and 839-1007 µm respectively). (g) zoom in the rectangle in (a). (h) zoom in the rectangle in (d). (i) profile plotted along the green line in (g) and (h), where increase of SNR in case of the 4 B-scans pOCTA can be verified. (j) improvement of SNR at three depths.

Biomedical Optics EXPRESS

All OCTA methods so far have in common, that they operate on multiple tomograms taken at the same location at the sample. Increasing the number of tomograms results in improved vascular contrast, but ultimately leads to longer recording times and the higher probability for motion artifacts. This is less of an issue for skin imaging or preclinical imaging, where the sample can be well stabilized. However, for some in-vivo situation such as in retinal imaging, or for real-time angiography display, it is desirable to achieve good contrast with a minimum of recorded tomograms. Spectrometer based OCT has been shown to exhibit low noise, such that angiography based on two tomograms yields already detailed vascular contrast. Swept source so far needs several images due to the intrinsic higher noise. Encouraged by the excellent phase stability of the akinetic source, we compare therefore the performance of OCTA based on 2 tomograms to OCTA based on four tomograms per measurement location. The left column of Fig. 6 show the resulting angiograms with 2 B-scans per position versus the angiograms at the same area employing four tomograms shown in the right column. As in the previous results, median z-projection and Gaussian filtering is employed. For better comparison, the angiograms have been normalized to the maximum value within the respective depth projections.

Figure 6(a), 6(b), 6(c) display *en-face* angiograms for pOCTA based on two B-scans per position at different depths (294-587 μm, 587-839 μm and 839-1007 μm respectively). Figure 6(d), 6(e), 6(f) demonstrate angiograms with pOCTA based on 4 B-scans at the same three depths, respectively. Figure 6(g) and Fig. 6(h) show zoomed regions indicated by the rectangles in Fig. 6(a) and Fig. 6(d). Figure 6(i) are profiles plotted along the yellow line in (g) and (h). According to Fig. 6(i), the peak signal from vessel cross-sections of the 4 B-scan protocol pOCTA are higher than 2 B-scans, as one would expect. According to Eq. (3), as section 3.4, we calculated an improvement of 2.15 dB in SNR for Fig. 6(d), as compared to Fig. 6(a); an improvement of 1.36 dB in SNR for Fig. 6(e), as compared to Fig. 6(b); an improvement of 1.32 dB in SNR for Fig. 6(f), as compared to Fig. 6(c). The improvement of SNR in three depth is shown in Fig. 6(j). The improvement in SNR comes at the expense of acquisition time by a factor of two. Despite the lower SNR, pOCTA based on 2 B-scans shows already excellent microvascular details as appreciated from Fig. 6.

Biomedical Optics EXPRESS

3.6 Comparison of narrow bandwidth laser (37 nm) with broad bandwidth laser (100 nm) using simple phase based OCT angiography

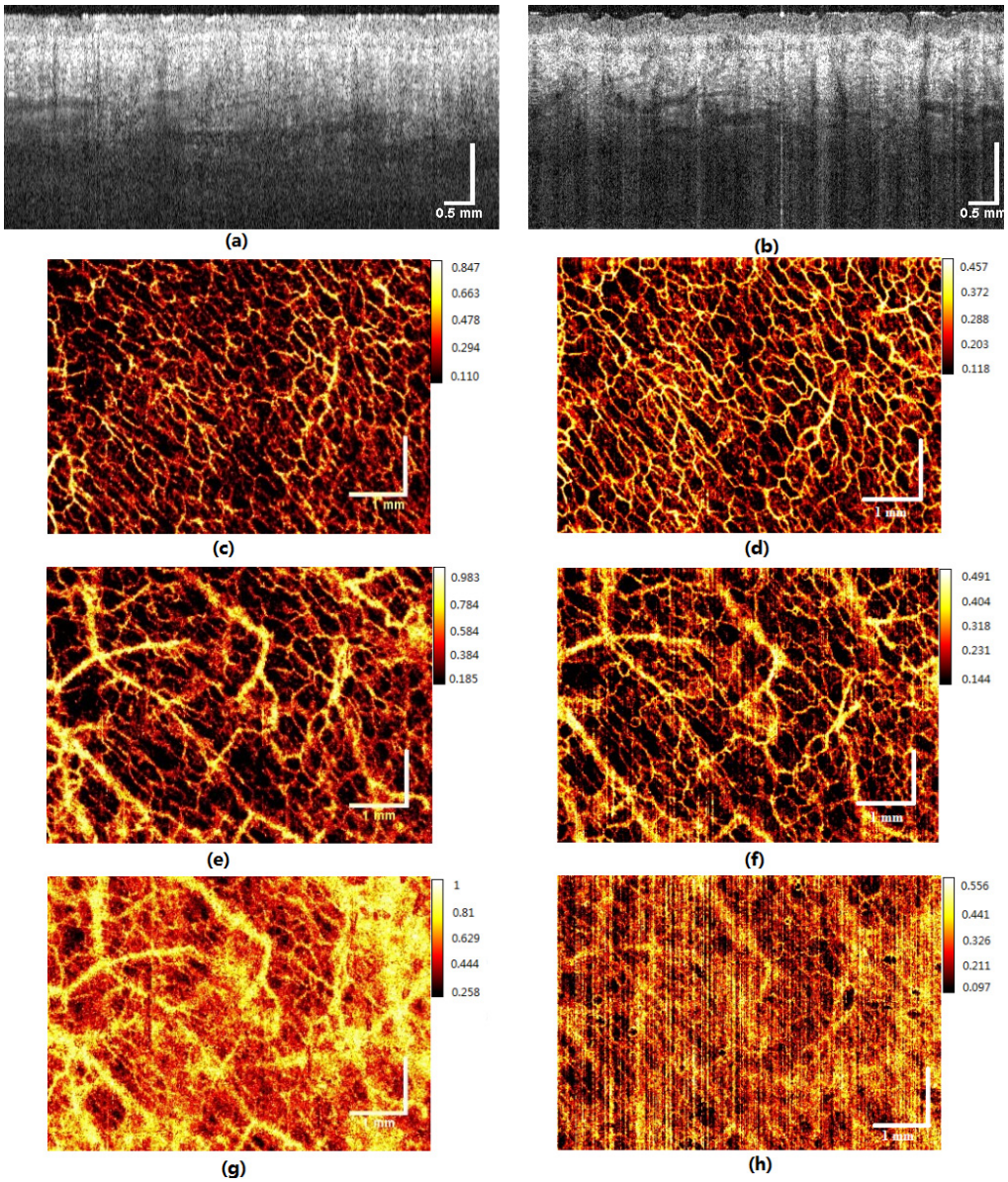

Fig. 7. Comparison of phase based OCTA using a narrow bandwidth (37 nm) and a broad bandwidth laser (100 nm). (a) tomogram (8 × 3.6 mm) obtained with the narrow bandwidth laser. (b) tomogram with the broad bandwidth laser (8 × 3.6 mm). (c), (e), (g) phase based angiograms using narrow bandwidth laser at different depths (294-587 μm, 587-839 μm and 839-1007 μm respectively), the size of all angiograms is 6.5 × 4.5 mm, 419 × 281 pixels. (d), (f), (h) phase based angiograms using broad bandwidth laser at different depths (294-587 μm, 587-839 μm and 839-1007 μm respectively).

The results before section 3.6 were acquired with an akinetic laser centered at 1340 nm and with 37 nm bandwidth. Due to the spectral profile of the tuned spectrum being close to rectangular (the intensity variation is within 0.015 dB), the optical bandwidth of the akinetic swept laser is equal to the tuned wavelength range, not the −3 dB width. Although the smaller

Biomedical Optics EXPRESS

bandwidth is beneficial for OCTA due to the higher stability with respect to motion artifacts, larger optical bandwidth and thus axial resolution would be desirable for OCT. Figure 7(b) demonstrates the performance of a first prototype akinetic laser at 1310 nm center wavelength with 100 nm bandwidth.

The performance of akinetic broad bandwidth laser for OCTA is demonstrated in the right column of Fig. 7(d), 7(f), 7(h), show three angiograms taken at three depths (294-587 µm, 587-839 µm and 839-1007 µm respectively). Figure 7(a), 7(c), 7(e), 7(g) compare the results to the narrow bandwidth laser at the same respective depths. All the angiograms employ median z-projection, Gaussian filtering with kernel pixel size 0.8. Two data sets were acquired at close to the same position at the hand palm using the narrow and broad bandwidth system, respectively. 20 minutes are necessary for changing the laser and preparation for the experiment. Therefore the sampling area and pressure at the hand palm are slightly changed between the two cases. For the broad bandwidth laser an axial resolution of 9.77 µm was measured. The better axial resolution is also well appreciated by comparing the tomograms in Fig. 7(a) and 7(b). With 6.0 mW on the sample, a sensitivity of 101 dB was measured for the broad bandwidth system, which was slightly lower than the small bandwidth system sensitivity of 103 dB.

Comparing the performance for OCTA, shows good microvascular contrast for both lasers for the upper layers. At larger depth, the higher resolution OCTA seems to be more prone to scattering artifacts, leading to strong contrast degradation.

A remaining challenge for future research is the persisting jitter noise using the broad bandwidth laser (100 nm) which is in addition responsible for the stripe artifacts visible in Fig. 7(h). Removal of this noise needs technological fine-tuning and better synchronization between the laser and the FPGA to remove spurious jitter noise.

4. Conclusion

We demonstrated an akinetic, all-semiconductor, highly phase-stable swept source laser for OCT and OCT angiography in human skin *in vivo*. It has been previously shown, that the laser based on akinetic tuning combines high instantaneous coherence length of several tens of centimeters with extremely high wavelength stability. The standard deviation of phase repeatability is less than 2 mrad. Furthermore, it produces low excess noise. Especially the tuning stability holds great promise for phase sensitive OCT modalities such as phase based OCTA and complex signal OCTA. Dedicated hardware such as fiber Bragg gratings, reference interferometers and sophisticated post-processing routines are not necessary anymore to ensure a wavelength-stable sampled signal, due to the extremely high phase linearity and phase repeatability. The akinetic swept source laser significantly simplifies the system regarding to hardware and the post-processing routines.

Using this highly phase-stable laser, the angiograms of human palm and fingernail region were presented. It demonstrated the capability for visualization of microvascular structures using phase sensitive OCTA .We further evaluated and compared the imaging performance of vascular networks delivered by two algorithms, speckle difference iOCTA and phase difference pOCTA. It is seen in accordance with previous work, that the pOCTA yields better contrast than speckle based OCTA in terms of SNR with increasing depth in strongly scattering media such as skin.

Due to the excellent phase stability, it is expected that a smaller number of tomograms for OCTA is sufficient to achieve good microvascular contrast similar to spectrometer based OCTA. We compared the performance of OCTA based on 2 B-scans per position and 4 B-scans per position. The results show, that 4 B-scans yield better SNR as 2 B-scans as is expected from the higher number of tomograms. However, capillary structures and vascular networks in the skin are already visualized impressively with high contrast using 2 B-scans. As already mentioned, higher measurement time for skin OCTA is less critical as for example for ocular OCTA, where involuntary motion artifacts are unavoidable. Also for real-time

Biomedical Optics EXPRESS

angiography display such as for intrasurgical applications, it is desirable to achieve good contrast with a minimum of recorded tomograms.

We finally presented first structural OCT images as well as OCTA with a broad bandwidth akinetic laser prototype with an axial resolution of 9.77 µm. The higher resolution leads to degradation of vascular contrast in depth, indicating that a smaller bandwidth is in general beneficial for OCTA.

The presented results demonstrate a remarkable potential of simple phase-stable swept source OCTA for structural and functional tissue imaging. We have finally reached a point that the akinetic swept source realizes swept source OCT with phase and noise performance, that can be well compared to spectrometer based OCT, being even superior with respect to coherence length and roll-off performance. It can be expected that the simple hardware design and phase stability will make it the laser source of choice for phase sensitive OCT applications, such as OCT elastography, quantitative Doppler OCT, or digital refocusing and aberration correction.

Funding

European Union projects FAMOS (FP7-ICT-217744); Austrian Science Fund (FWF) (P26687).

Acknowledgments

We thank Elisabet Rank for carefully proofreading the paper, and Behrooz Zabihian for his kind support with ImageJ.